

Computational Fluid Dynamics and Aortic Thrombus Formation Following Thoracic Endovascular Aortic Repair

Foeke J. H. Nauta, MD, PhD, Kevin D. Lau, PhD, Christopher J. Arthurs, PhD, Kim A. Eagle, MD, David M. Williams, MD, Santi Trimarchi, MD, PhD, Himanshu J. Patel, MD, and Carlos A. Figueroa, PhD

Departments of Surgery, Biomedical Engineering, Internal Medicine, Radiology, and Cardiac Surgery University of Michigan, Ann Arbor, Michigan; Thoracic Aortic Research Center, Vascular Surgery, Policlinico San Donato IRCCS, University of Milan, Italy; and Division of Imaging Sciences and Biomedical Engineering, King's College London, London, United Kingdom

Background. We present the possible utility of computational fluid dynamics in the assessment of thrombus formation and virtual surgical planning illustrated in a patient with aortic thrombus in a kinked ascending aortic graft following thoracic endovascular aortic repair.

Methods. A patient-specific three-dimensional model was built from computed tomography. Additionally, we modeled 3 virtual aortic interventions to assess their effect on thrombosis potential: (1) open surgical repair, (2) conformable endografting, and (3) single-branched endografting. Flow waveforms were extracted from echocardiography and used for the simulations. We used the computational index termed platelet activation potential (PLAP) representing accumulated shear rates of fluid particles within a fluid domain to assess thrombosis potential.

Results. The baseline model revealed high PLAP in the entire arch (119.8 ± 42.5), with significantly larger PLAP at the thrombus location (125.4 ± 41.2 , $p < 0.001$). Surgical

repair showed a 37% PLAP reduction at the thrombus location (78.6 ± 25.3 , $p < 0.001$) and a 24% reduction in the arch (91.6 ± 28.9 , $p < 0.001$). Single-branched endografting reduced PLAP in the thrombus region by 20% (99.7 ± 24.6 , $p < 0.001$) and by 14% in the arch (103.8 ± 26.1 , $p < 0.001$), whereas a more conformable endograft did not have a profound effect, resulting in a modest 4% PLAP increase (130.6 ± 43.7 , $p < 0.001$) in the thrombus region relative to the baseline case.

Conclusions. Regions of high PLAP were associated with aortic thrombus. Aortic repair resolved pathologic flow patterns, reducing PLAP. Branched endografting also relieved complex flow patterns reducing PLAP. Computational fluid dynamics may assist in the prediction of aortic thrombus formation in hemodynamically complex cases and help guide repair strategies.

(Ann Thorac Surg 2016;■:■-■)

© 2016 by The Society of Thoracic Surgeons

The feasibility of thoracic endovascular aortic repair (TEVAR) is profusely being explored in the aortic arch and ascending aorta [1, 2]. Nevertheless, important postoperative complications are reported, with high rates of reintervention [3, 4]. This may be attributable to the considerable more complex hemodynamics (ie, non-laminar flow and high velocities) in the proximal thoracic aorta when compared with the descending or abdominal aorta. Over-stenting of the left subclavian artery, which is often performed to provide a good proximal landing zone, might modify flow patterns within the aortic arch. This remains to be determined, however. To optimize endograft design and treatment outcomes, it is timely to seek a deeper understanding of hemodynamics following proximal TEVAR.

Computational fluid dynamics (CFD) has been used increasingly in the last decade for the investigation of cardiovascular diseases and surgical planning [5, 6]. The so-called “image-based modeling” paradigm of CFD uses anatomical data obtained from computed tomography angiography (CTA) or magnetic resonance imaging (MRI) to create a three-dimensional computational

Drs Eagle and Patel disclose financial relationships with WL Gore Inc, Medtronic, and Terumo; Dr Williams with WL Gore Inc and Boston Scientific; Dr Trimarchi with WL Gore Inc and Medtronic; Dr Figueroa with Bolton Medical and Aneumed, Inc.

The Video can be viewed in the online version of this article [<http://dx.doi.org/10.1016/j.athoracsur.2016.09.067>] on <http://www.annalsthoracicsurgery.org>.

Accepted for publication Sept 19, 2016.

Address correspondence to Dr Figueroa, Departments of Surgery and Biomedical Engineering, University of Michigan, 431 S First St, Ann Arbor, MI 48103 USA MI; email: figueroa@med.umich.edu.

model representing the blood vessels of interest. Additional physiological measurements of flow, pressure, and wall motion are used to inform the “boundary conditions” of the simulation. Computational analyses of these models provide detailed descriptions of hemodynamic quantities such as velocity and pressure, but also of additional hemodynamic quantities including wall shear stress, oscillatory shear stress, displacement forces, and so forth. Recent CFD developments allow for the tracking of virtual “blood particles”, which gives insight into blood flow patterns and the pathlines of these particles. Recently, a metric termed the platelet activation potential (PLAP) has been proposed [6, 7]. This metric calculates the shear rates that a fluid particle accumulates during its travel in the blood stream, therefore providing an insight into potential platelet activation. The role of platelet activation in high shear flows has been recognized in the genesis of arterial thrombus [8]. We thus use the PLAP index to investigate correlation between high platelet activation and localization of aortic thrombus by means of computational analyses performed in a patient presenting with ascending aortic thrombus following TEVAR. Different virtual surgical and endovascular repairs will be assessed to study its impact on hemodynamics and on PLAP.

Patients and Methods

Clinical Data

CTA was performed with 64-slice scanners and intravenous injection of 80 to 120 mL of nonionic iodinated contrast material. The CTA was used to build the computational models. MRI studies were conducted using a gadolinium-based contrast agent (gadobenate dimeglumine) and steady-state free precession cine imaging. Additionally, black blood imaging and multiphase dynamic three-dimensional MRI were performed with the injection of the contrast bolus to visualize aortic thrombus. Approval was obtained from the institutional review board, and the need for informed consent was waived. The patient’s medical charts were reviewed to retrieve information on demographics, medical and surgical history, and clinical outcome.

Patient History

A 74-year-old female patient presented with ascending aortic thrombus following TEVAR for growing aneurysm of the distal aortic arch (Fig 1). Her surgical history included an uneventful ascending and arch repair for ascending aneurysm 3 years prior to presentation (Fig 1A). Postoperatively, a mild kink was observed in the surgical graft in the inner-curvature of the ascending aorta, which was left untreated (Fig 1B). She was a nonsmoker with a history of hypertension, chronic obstructive pulmonary disease, and congestive heart failure, with a NYHA score of I. The patient was not known to have any hematologic disorder. Her blood pressures were stable around 125/80 mm Hg with

antihypertensive medication and a regular heart rate of about 80 to 90 beats per minute. She had no symptoms relevant to her aortic disease (no back pain, shortness of breath, or palpitations). A paraanastomosis aneurysm dilatation was observed 3 years postoperatively (Fig 1C), which was treated with a TEVAR procedure, following a left carotid-subclavian artery bypass with embolization of the proximal left subclavian artery (LSA, Fig 1D). Three overlapping Medtronic Valiant (Medtronic Vascular, Santa Rosa, CA) thoracic endografts were implanted (36 x 36 x 200 mm Freeflow, 36 x 36 x 200 mm closed, and 36 x 36 x 160 mm). Her postoperative course was uneventful. Follow-up angiography demonstrated seal without endoleak. One month follow-up CTA imaging revealed a linear irregular area of low-attenuation within the lumen of the distal ascending aorta at the proximal landing zone of the endograft concerning for intraluminal thrombus. Maximum aortic diameter was 56 mm at the upper descending thoracic aorta within the stented segment. Intravascular ultrasound demonstrated intraluminal, echogenic, and mobile material within the aortic lumen at the bare metal end of the proximal endograft, presumed to be thrombus. MRI confirmed ascending aortic thrombus at the proximal endograft end and a kink in the aortic arch region (Figs 1E, 1F). Patient was started on warfarin tablet of 2.5 mg daily. She had a Thrombosis Risk Assessment or Caprini score of 9. Her blood pressure at time of MRI imaging was 133/77 mm Hg with a regular heart rate of 67 beats per minute. Transthoracic echocardiography measured a cardiac output of 4.87 L/min with a normal left ventricular systolic function and an ejection fraction of 60%. No relevant valve disease or any intracardiac thrombus was observed.

Patient-Specific Computational Modeling

First, a patient-specific computational model describing the aortic morphology post-TEVAR was built. Additionally, we built 3 virtual surgical and endovascular repair models that seek to alter hemodynamics in such a way as to remove the aortic thrombus: (1) a surgical repair of the ascending aorta eliminating the kink in the graft, (2) a conformable endograft in the arch reducing the kink in the arch, and (3) a single-branched endograft restoring perfusion into the LSA (Fig 2).

Each computational model consists of (1) a three-dimensional geometric model of the thoracic aorta, the coronaries, and the upper arch branches, and (2) a set of boundary conditions that represent the physiological variations of the patient’s pressure and flow. The geometric models were built based on the CTA image data using a three-dimensional path-planning approach in the software package CRIMSON [9]. A finite element mesh, consisting of about 1.4 million tetrahedral elements, was created for each model. Mesh adaptation and curvature refinement were used to increase the resolution in regions of high velocities and complex flow. The vessel walls were modeled as rigid. Our workflow consisted of first building a baseline model, which was used to match the patient-specific hemodynamics through the

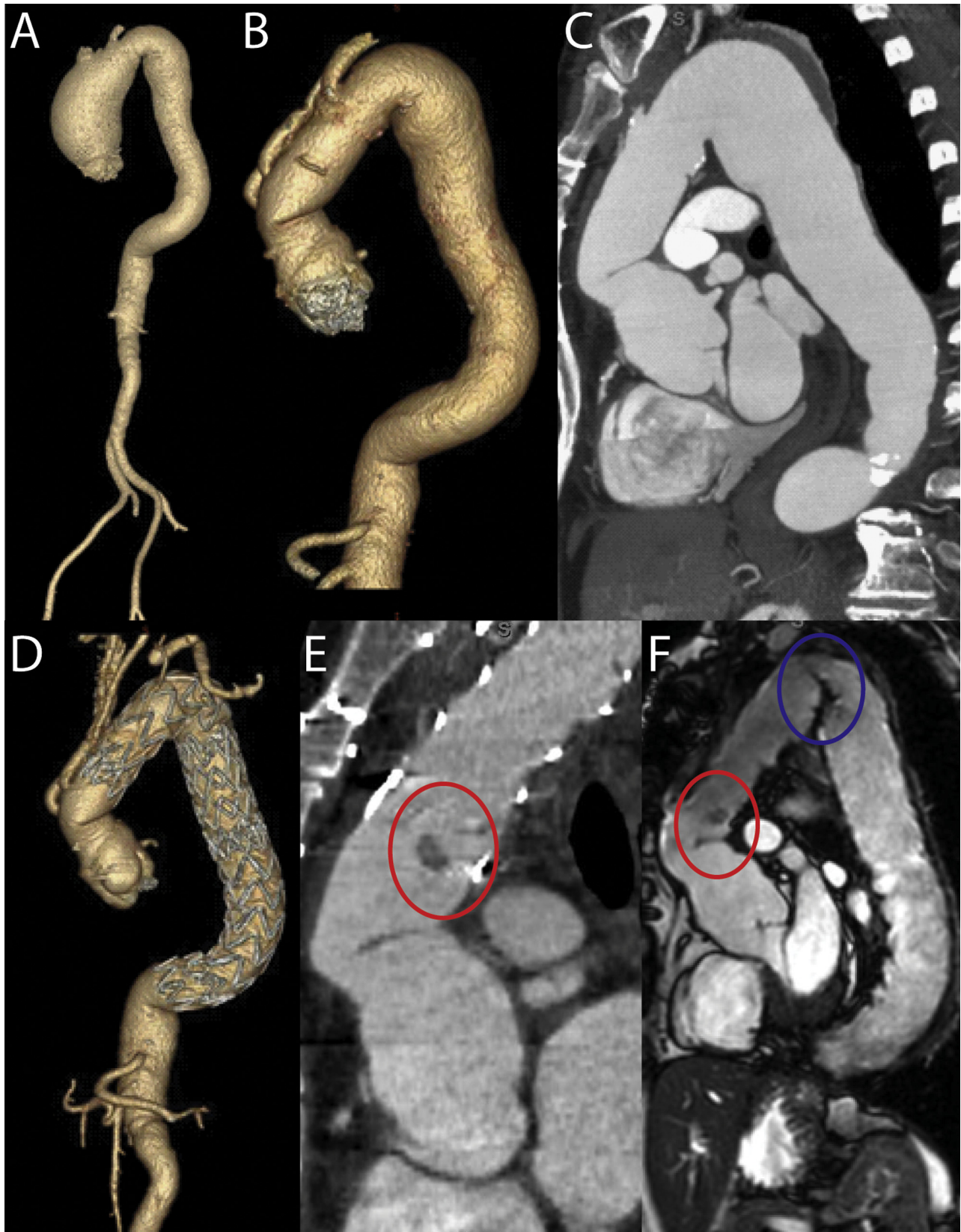


Fig 1. Patient history showing (A) ascending aortic aneurysm which was repaired with a (B) surgical graft in 2012. (C) Paraanastomosis aneurysm dilatation 3 years postoperatively, which was treated with (D) TEVAR in December 2015. (E) Computed tomography angiography 1 month post-TEVAR suggested intraluminal thrombus at the proximal endograft end, as indicated by the red circle. (F) Magnetic resonance imaging confirmed ascending aortic thrombus, as marked by the red circle. The kink in the endograft is denoted with the blue circle. (TEVAR = thoracic endovascular aortic repair.)

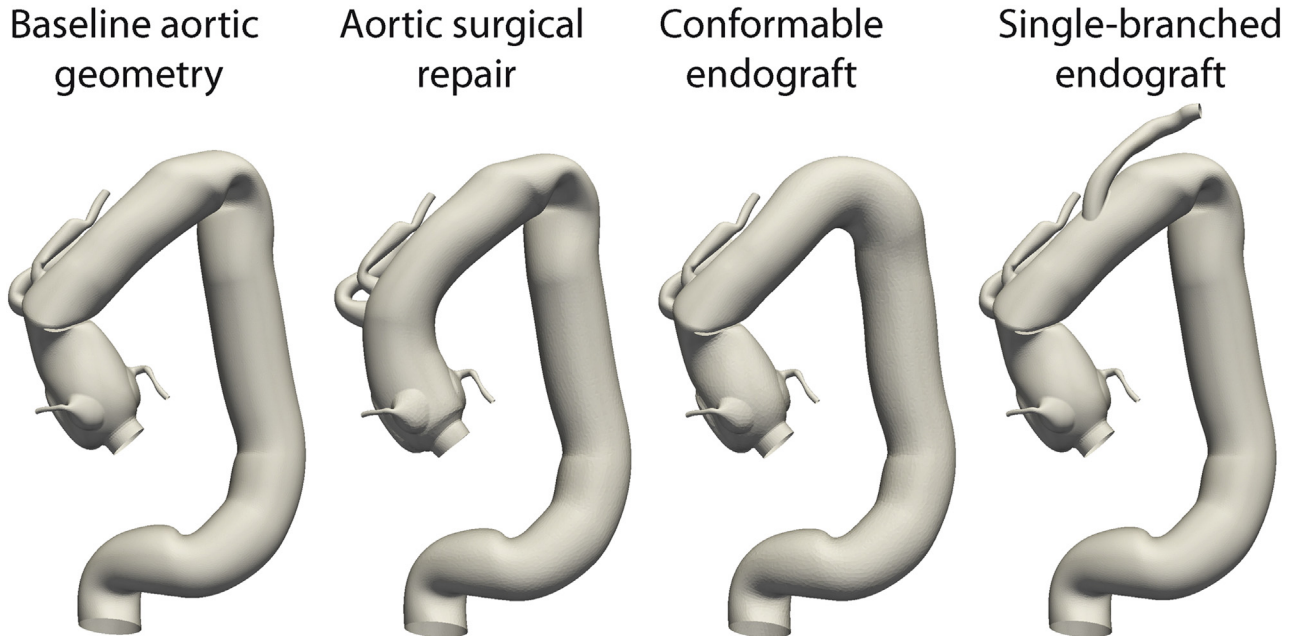


Fig 2. Models of the different aortic geometries. From left to right: the baseline aortic geometry, the ascending aortic surgical repair, the conformable endograft, and the single-branched endograft into the LSA. (LSA = left subclavian artery.)

fine-tuning of lumped parameter Windkessel models at the aortic outlets (Fig 3), a heart model [10], and lumped-parameter coronary models [11]. The use of a heart model and of coronary models was important to correctly represent hemodynamics in the ascending aorta as diastolic coronary perfusion has an important impact on local flow patterns [12].

Each Windkessel model represents the vasculature distal to its outlet and consists of a proximal resistance, a compliance, and a distal resistance. The sum of proximal and distal resistances of each branch was tuned through an iterative procedure to match the patient's mean pressure of 96 mm Hg and reference flow splits [13, 14]. The tuning ensured that flow to the innominate artery was about 18% of cardiac output, and about 8% of cardiac output was appointed to the LSA, 8% to the left common carotid artery, and 60% to the thoracic outlet. The coronary lumped parameter models were adjusted such that each coronary received about 3% of the cardiac output [13, 14].

To represent the increase in flow in the left carotid-subclavian artery bypass, the LSA target share of the total flow was added to that of the left common carotid artery for the baseline aortic, the ascending aortic surgical repair, and the conformable endograft models. The compliance of each Windkessel model was tuned to reproduce the patient's pulse pressure of 56 mm Hg. The velocity profile imposed at the aortic root was created using the volumetric flow waveform digitalized from the patient's transthoracic echocardiography data. Blood was modeled as a Newtonian fluid with a density of $1,060 \text{ kg/m}^3$ and a dynamic viscosity of $0.004 \text{ Pa} \cdot \text{s}$. No-slip wall boundary conditions were enforced on the wall of the model.

The flow and pressure waveforms in Figure 3 highlight physiologically realistic profiles, including diastolically dominant left coronary artery flow, increased diastolic flow in the right coronary artery, patient-matched values of pulse pressure, and target values of flow splits between the different vessels.

Particle Tracking and Platelet Activation Potential

Our primary interest was in the estimation of regions of high shear within the aortic lumen that could lead to high platelet activation, flow recirculation, and eventually thrombus formation. Another factor affecting thrombus deposition is endothelial inflammation, a circumstance that is known to occur in the presence of disturbed flows and flow stasis. In this case, however, the native ascending aortic tissue was replaced by a surgical Dacron graft in which no endothelial cells are present. Therefore, aortic thrombosis in this patient was assumed to be predominantly driven by platelet activation. We expected the kinked Dacron graft to result in nonlaminar flow patterns leading to prolonged mechanical stimulation of blood platelets, which is known to increase the risk of thrombosis [15, 16]. To quantify this we used a CFD tool named 'particle tracking' which allows evaluation of the history of shear rate that a particle experiences along its path within a fluid. We injected 1.3 million particles into the aortic root and collected flow-induced shear rates for each particle at each time step using a Lagrangian particle-tracking technique [6]. Full details on this method have been reported previously [6]. These data were used to quantify PLAP, a dimensionless scalar index that represents accumulated shear rates that have been associated with thrombosis [6, 7]. Data on PLAP were subsequently

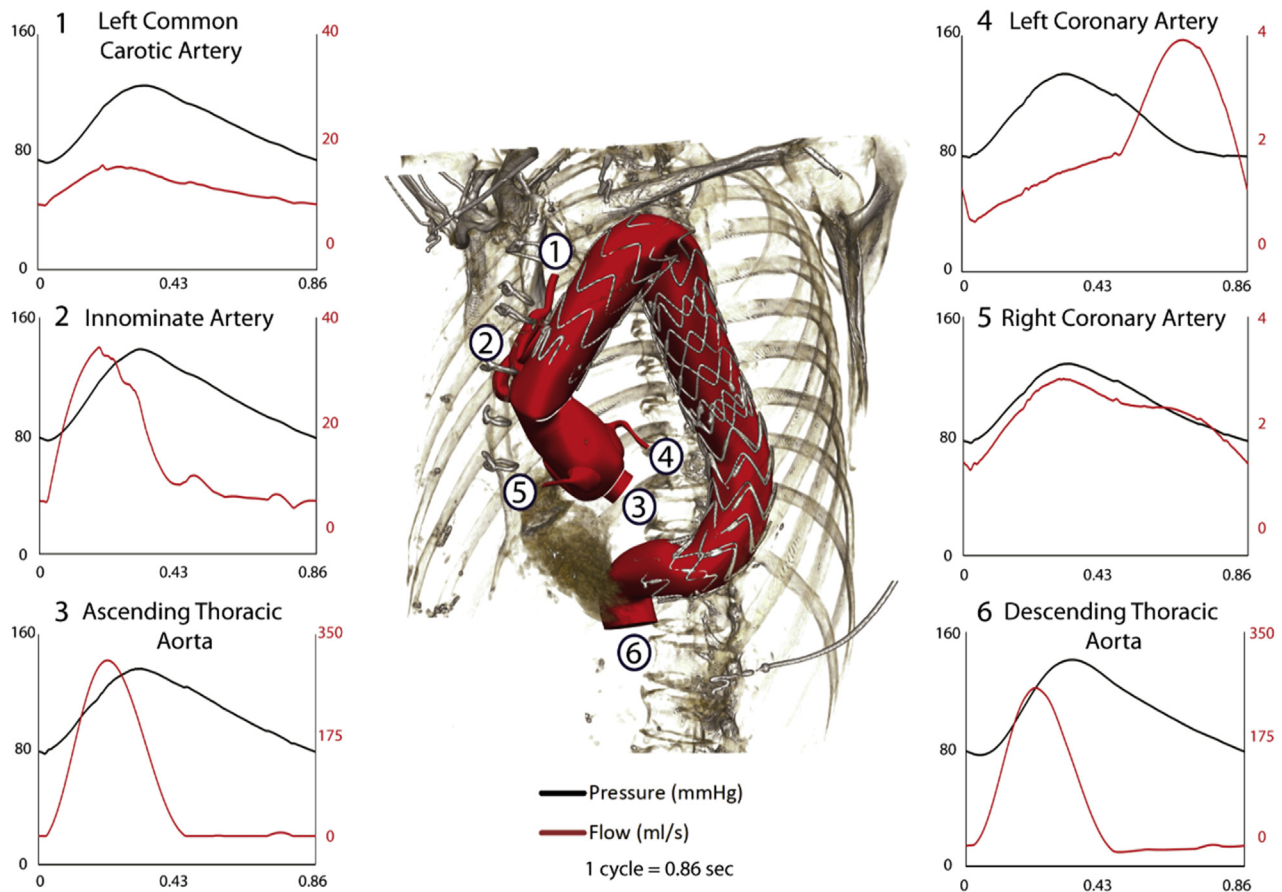


Fig 3. Pressure (black lines) and flow waveforms (red lines) computed at thoracic aorta inflow and different branch outlets. The location of each measurement is denoted by a number.

collected for each particle after two cardiac cycles. Two standardized regions of interest (ROIs) were used for all models in which to define PLAP: (1) the region stretching from the kink to the aortic arch, and (2) the specific location of thrombus as identified in CTA and MRI imaging data (Fig 4).

Statistical Analyses

Data were analyzed with SPSS 23.0 (SPSS, Chicago, IL) and are presented as mean \pm standard deviation, where applicable. Statistical analyses of differences between models were performed using one-way analysis of variance testing for means of PLAP over all particles present in the ROI at the end of the second cardiac cycle after particle release. Normal distribution of the PLAP data was assessed by skewness and kurtosis Z-values between -1.96 and 1.96 , the Shapiro-Wilk test p -value above 0.05 , and visualization of approximately normally distributed data with histograms. All p -values less than 0.05 were considered statistically significant.

Results

The computed hemodynamics of the baseline model are summarized in Figure 3. Peak flow was 304.7 mL/s and

254.2 mL/s in the ascending and descending aorta, respectively. Retrograde diastolic flow was observed in both ascending (with a peak of 0.2 mL/s) and descending aorta (peak of 25.8 mL/s). The different flow and pressure waveforms show realistic profiles for all branches of the model, including predominantly diastolic flow in the left coronary artery, matched mean values of pressure and flows, as well as pulse pressure. These waveforms therefore ensure a physiologically realistic distribution of pulsatile velocities in the aorta, which can then be used to examine the shear activation state of particles traveling through the blood stream.

Two cardiac cycles following virtual particle injection revealed significant differences in PLAP among the different models (Fig 4; Video).

Baseline Model

The baseline model presented disturbed flow patterns at the location of the surgical kinked graft and high rates of PLAP in the ROI just distal to the graft kink and corresponding with the exact location of aortic thrombus (Figs 4A, 4B). This resulted in PLAP values in the entire aortic arch ROI of 119.8 ± 42.5 , and statistically significant larger values of PLAP in the thrombus ROI (125.4 ± 41.2 , $p < 0.001$).

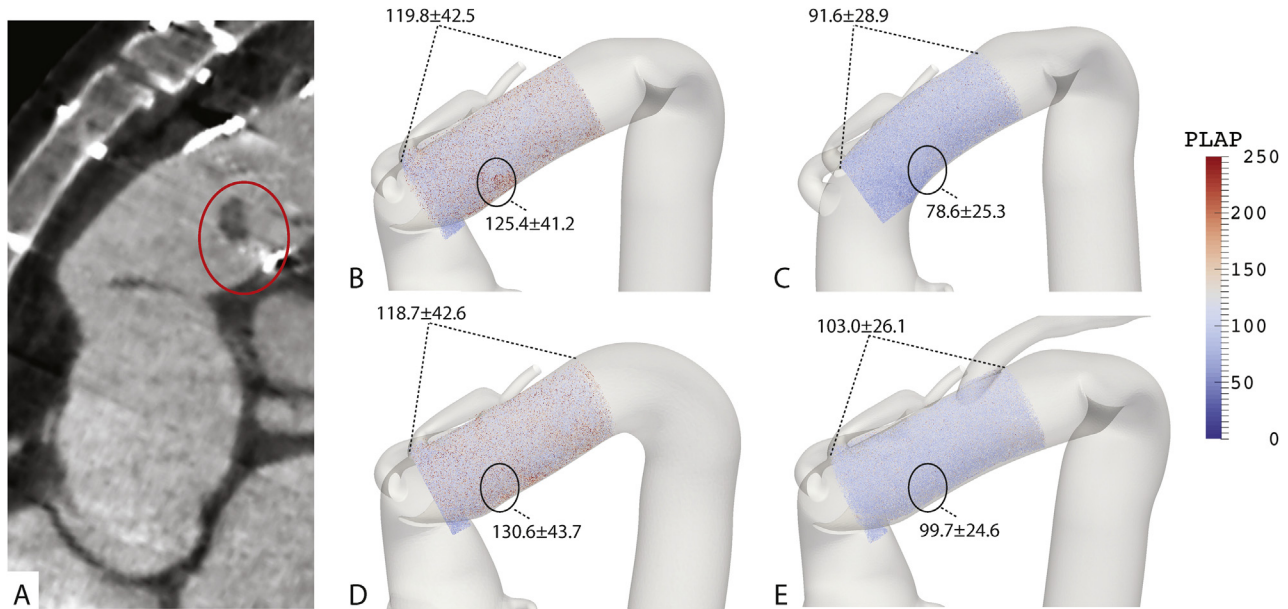


Fig 4. (A) Computed tomography imaging showing the aortic thrombus (red circle). (B–E) Particles and their corresponding PLAP value are shown at the end of the second cardiac cycle. Average PLAP are given for each model for both the aortic arch ROI (denoted within the two dashed lines) as well as for the thrombus location ROI (marked with a black circle). (B) Baseline aortic geometry, (C) aortic surgical repair, (D) conformable endograft, and (E) single-branched endograft. One-way analysis of variance testing calculated $p < 0.001$ for PLAP differences among the four models in both ROI. See the Online Video for a dynamic visualization of PLAP in each model. Values are presented as mean \pm SD. (PLAP = platelet activation potential; ROI = region of interest.)

Surgical Repair Model

When assessing hemodynamics in the virtual surgical repair model a significant 24% drop in mean PLAP was noted in the aortic arch ROI (91.6 ± 28.9 , $p < 0.001$) and a 37% drop (78.6 ± 25.3 , $p < 0.001$) at the thrombus ROI (Fig 4 C). This result suggests that the kink in the surgical Dacron graft is behind the significant hemodynamic alterations in the aortic arch and that it critically contributed to the formation of thrombus.

Conformable Endograft Model

This design did not have a profound effect on PLAP, resulting in a modest 4% increase in PLAP (130.6 ± 43.7 , $p < 0.001$) in the thrombus ROI relative to the baseline case, and an even smaller 1% change in the aortic arch ROI (118.7 ± 42.6 , $p < 0.001$) (see Fig 4D). This suggests that the effect of the distal endograft kink on thrombus formation in the Dacron graft region is minimal.

Single-branched Endograft

PLAP was significantly reduced in the single-branched endograft model in comparison with the baseline model. The aortic arch ROI exhibited a 14% drop in PLAP (from 119.8 ± 42.5 to 103.0 ± 26.1 , $p < 0.001$) and 20% drop in PLAP at the thrombus ROI (125.4 ± 41.2 to 99.7 ± 24.6 ; Fig 4E). These results suggest that, although the changes in hemodynamics (particularly in blood shear) relative to the baseline model are not as profound as in the

surgical repair graft, they could lead to a situation in which thrombus would not have formed.

Clinical Follow-up

An 18-week follow-up CTA-scan demonstrated that the thrombus volume remained stable (Fig 5). Patient was continued on warfarin tablets of 2.5 mg daily.

Comment

This study demonstrated a correlation between intraluminal ascending aortic thrombus and high levels of intraluminal shear through CFD analysis. Complex flow

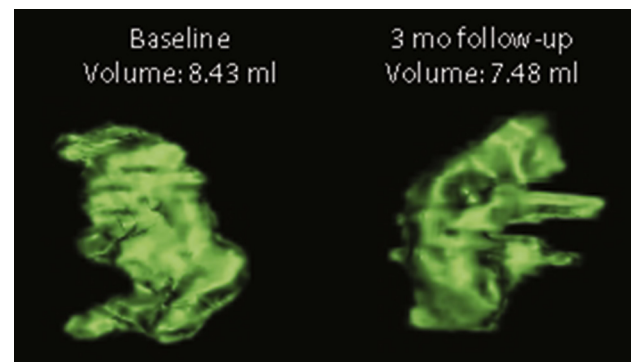


Fig 5. Computed tomography at baseline and at 18 weeks follow-up demonstrating stable three-dimensional volumes of the intraaortic thrombus.

patterns in a complex geometry resulting from kinking of a vascular graft appear to significantly contribute to the increase in shear rates between blood particles. Such shear is known to activate platelets with altered risk of thrombus formation [6, 7]. This study had two primary motivations: (1) to confirm the suitability of the platelet activation potential metric in identifying potentially high-risk locations for thrombus formation, and (2) to assess the efficacy of different virtual surgical and endovascular repairs to minimize the state of high shear observed the baseline kinked aortic geometry.

The high PLAP value in the baseline model suggests that complex flow patterns, caused by the severely kinked Dacron graft in the ascending aorta, are associated with increased shear rates between particles. The hotspot of elevated PLAP matched the location of aortic thrombus at the proximal end of the endograft accurately, which highlights the potential added value of this quantification. More broadly, our findings stress the fundamental relationship between fluid mechanic pathways for platelet activation and disturbance of blood flow patterns due to surgical interventions.

Typically, thrombus formation occurs along the aortic wall. In case of pathologic or surgically modified vessels, however, fluid stresses may be so severe that platelets are activated even in high-speed velocity fields, such as in the case presented here. This emphasizes the potential risks of geometric alterations in the natural curvature of the proximal thoracic aorta. It appears that it is the high tortuosity of the endograft itself that triggers thrombus formation, as reported in a canine model showing intraluminal thrombus 2 months following endografting [17]. Furthermore, surgical Dacron grafts have been shown to induce intraluminal thrombus, in particular at the anastomosis site. This has been thought to be caused by the lower mechanical compliance of the graft versus the native aorta, which generates a disturbed flow pattern promoting neointimal hyperplasia [18, 19]. These mechanisms, in combination with high intraluminal shear, may have contributed to the thrombus formation in the patient presented in this study.

The different surgical repairs examined in this paper produced distinct hemodynamic regimes in the ascending aorta. PLAP was significantly reduced following virtual surgical repair of the ascending aorta. It appears that restoration of normal flow patterns considerably reduces the shear rate between blood particles. This result demonstrates the predictive and adjunctive value of CFD in planning aortic surgery. Conversely, elimination of the second kink in the endografted aortic arch did not result in improvements of PLAP in the segment of aortic thrombus. This result was expected as the distal kink was not severely stenotic and was located at a considerable distance from the thrombus region and thus had little effect on local flow disturbances. Lastly, we did find that the virtual single-branched endograft with extension into the LSA reduced PLAP significantly in both the entire aortic arch but specifically in the region where thrombus was present. This result suggests that high shear rates may be relieved downstream of the stenotic flow

disturbance by enabling the natural conduit of the LSA by means of a branched endograft solution. Even though the reduction in PLAP is not as large as with the virtual surgical repair that eliminates the kink in the Dacron graft, its advantages over the baseline case are clear. In fact, this finding may have led to the consideration of fenestrating the implanted thoracic endograft with a laser to restore LSA blood perfusion [20]. Nonetheless, the LSA was embolized in this particular case which precluded the potential to restore LSA perfusion.

These results further emphasize the added value of CFD analysis in the planning of complex endovascular aortic repairs [5, 21].

Limitations

The main limitation of this study is the small sample size. The described computational analyses aimed at presenting and evaluating a recently introduced hemodynamic metric for thrombus formation in high-speed velocity fields. This was performed using a patient-specific case to illustrate its potential value. Larger sample sizes are needed to validate the predictive value of PLAP for thrombus formation. Furthermore, a combination of high shear and high residence time could lead to additional computational metrics with stronger correlation with thrombus localization. Ideally, a surgical or single-branched endograft repair would have been conducted on this patient to compare our computational predictions with in vivo clinical follow-up data. Nevertheless, this patient was managed nonoperatively. This pilot study may motivate further research to confirm the utility of CFD in predicting intraluminal thrombus potential and the feasibility of reversing increased platelet activation through aortic intervention.

Conclusion

CFD enriches the analysis of hemodynamics in complex pathologic aortic geometries. In this study we presented the added value of particle tracking and evaluation to quantify the potential risk of intraluminal thrombus. Particles that have accumulated a high shear history are susceptible to clot and cause thrombus, even in the high velocities of the ascending aorta. Additionally, CFD offers the assessment of virtual surgical or endovascular repairs on a metric of interest. We found that virtual surgical repair of the ascending aorta reduced flow complexity and simulated platelet activation considerably. Moreover, the use of a virtual branched endograft that restored flow through the overstented LSA also decreased shear rates between particles. These findings may have implications for endograft design as they underline the importance preservation of flow through the upper arch branches. Finally, this analysis motivates further research on the complex hemodynamics following endograft repair, for which CFD provides a promising tool.

The authors gratefully acknowledge financial support from the European Research Council under the European Union's Seventh Framework Programme (FP/2007-2013)/ERC Grant Agreement No. 307532, the Edward B. Diethrich Professorship, and the

Frankel Cardiovascular Center. Funding sources also include the Joe D. Morris Professorship, David Hamilton Fund, and the Phil Jenkins Breakthrough Fund.

References

- Piffaretti G, Galli M, Lomazzi C, et al. Endograft repair for pseudoaneurysms and penetrating ulcers of the ascending aorta. *J Thorac Cardiovasc Surg* 2016;151:1606–14.
- Khoynezhad A, Donayre CE, Walot I, Koopmann MC, Kopchok GE, White RA. Feasibility of endovascular repair of ascending aortic pathologies as part of an FDA-approved physician-sponsored investigational device exemption. *J Vasc Surg* 2016;63:1483–95.
- Faure EM, Canaud L, Marty-Ané C, Alric P. Hybrid aortic arch repair for dissecting aneurysm. *J Thorac Cardiovasc Surg* 2016;152:162–8.
- Canaud L, Ozdemir BA, Patterson BO, Holt PJE, Loftus IM, Thompson MM. Retrograde aortic dissection after thoracic endovascular aortic repair. *Ann Surg* 2014;260:389–95.
- Prasad A, Xiao N, Gong X-Y, Zarins CK, Figueroa CA. A computational framework for investigating the positional stability of aortic endografts. *Biomech Model Mechanobiol* 2013;12:869–87.
- Di Achille P, Tellides G, Figueroa CA, Humphrey JD. A haemodynamic predictor of intraluminal thrombus formation in abdominal aortic aneurysms. *Proc R Soc A Math Phys Eng Sci* 2014;470(2172).
- Shadden SC, Hendabadi S. Potential fluid mechanic pathways of platelet activation. *Biomech Model Mechanobiol* 2013;12:467–74.
- Casa L, Deaton D, Ku D. Role of high shear rate in thrombosis. *J Vasc Surg* 2015;61:1068–80.
- CRIMSON. The software for cardiovascular modelling and simulation. n.d. www.crimson.software.
- Lau KD, Figueroa CA. Simulation of short-term pressure regulation during the tilt test in a coupled 3D-0D closed-loop model of the circulation. *Biomech Model Mechanobiol* 2015;14:915–29.
- Arthurs CJ, Lau KD, Asrress KN, Redwood SR, Figueroa CA. A mathematical model of coronary blood flow control: simulation of patient-specific three-dimensional hemodynamics during exercise. *Am J Physiol Heart Circ Physiol* 2016;310:H1242–58.
- Scalia GM, Greenberg NL, McCarthy PM, Thomas JD, Vandervoort PM. Noninvasive assessment of the ventricular relaxation time constant (τ) in humans by doppler echocardiography. *Circulation* 1997;95:151–5.
- Lantz BM, Foerster JM, Link DP, Holcroft JW. Regional distribution of cardiac output: normal values in man determined by video dilution technique. *AJR Am J Roentgenol* 1981;137:903–7.
- Coogan JS, Humphrey JD, Figueroa CA. Computational simulations of hemodynamic changes within thoracic, coronary, and cerebral arteries following early wall remodeling in response to distal aortic coarctation. *Biomech Model Mechanobiol* 2013;12:79–93.
- Shankaran H, Alexandridis P, Neelamegham S. Aspects of hydrodynamic shear regulating shear-induced platelet activation and self-association of von Willebrand factor in suspension. *Blood* 2003;101:2637–45.
- Nobili M, Sheriff J, Morbiducci U, Redaelli A, Bluestein D. Platelet activation due to hemodynamic shear stresses: damage accumulation model and comparison to in vitro measurements. *ASAIO J* 54:64–72.
- Kim HB, Choi YH, So YH, et al. Tissue responses to endovascular stent grafts for saccular abdominal aortic aneurysms in a canine model. *J Korean Med Sci* 2012;27:1170–6.
- Moreno MJ, Aji A, Mohebbi-Kalhari D, Rukhlova M, Hadjizadeh A, Bureau MN. Development of a compliant and cytocompatible micro-fibrous polyethylene terephthalate vascular scaffold. *J Biomed Mater Res B Appl Biomater* 2011;97:201–14.
- Tiwari A, Kidane A, Salacinski H, Punshon G, Hamilton G, Seifalian AM. Improving endothelial cell retention for single stage seeding of prosthetic grafts: use of polymer sequences of arginine-glycine-aspartate. *Eur J Vasc Endovasc Surg* 2003;25:325–9.
- Redlinger RE, Ahanchi SS, Panneton JM. In situ laser fenestration during emergent thoracic endovascular aortic repair is an effective method for left subclavian artery revascularization. *J Vasc Surg* 2013;58:1171–7.
- Figueroa CA, Taylor CA, Chiou AJ, Yeh V, Zarins CK. Magnitude and direction of pulsatile displacement forces acting on thoracic aortic endografts. *J Endovasc Ther* 2009;16:350–8.